Full Paper

CONTRAST MEDIA & MOLECULAR IMAGING

Received: 17 July 2014, Revised: 9 October 2014, Accepted: 10 October 2014, Published online in Wiley Online Library

(wileyonlinelibrary.com) DOI: 10.1002/cmmi.1633

Ultrasmall particles for Gd-MRI and ^{68}Ga-PET dual imaging

Charles Truillet[a], Penelope Bouziotis[b], Charalambos Tsoukalas[b], Jérémy Brugière[a], Matteo Martini[a], Lucie Sancey[a], Thomas Brichart[a], Franck Denat[c], Frédéric Boschetti[d], Ulrich Darbost[e], Isabelle Bonnamour[e], Dimitris Stellas[f], Constantinos D. Anagnostopoulos[g], Vassilis Koutoulidis[h], Lia A. Moulopoulos[h], Pascal Perriat[i], François Lux[a]* and Olivier Tillement[a]

Nanoparticles made of a polysiloxane matrix and surrounded by 1,4,7,10-**tetraazacyclododecane-1-glutaric anhydride-4,7,10-triacetic acid (DOTAGA)[Gd^{3+}] and 2,2′-(7-(1-carboxy-4-((2,5-dioxopyrrolidin-1-yl)oxy)-4-oxobutyl)-1,4,7-triazonane-1,4-diyl)diacetic acid) NODAGA[$^{68}Ga^{3+}$] have been synthesized for positron emission tomography/magnetic resonance (PET/MRI) dual imaging. Characterizations were carried out in order to determine the nature of the ligands available for radiolabelling and to quantify them. High radiolabelling purity (>95%) after ^{68}Ga labelling was obtained. The MR and PET images demonstrate the possibility of using the nanoparticles for a combined PET/MR imaging scanner. The images show fast renal elimination of the nanoparticles after intravenous injection.Copyright © 2014 John Wiley & Sons, Ltd.**

Additional supporting information may be found in the online version of this article at the publisher's web site.

Keywords: multimodal imaging; PET/MRI; nanoparticles

1. INTRODUCTION

Medical diagnostics has been getting more and more reliable by the combination of data issued from multiple assays (1). Multimodal imaging is a powerful method that can provide accurate detection of disease site (2), because the disadvantages of poor temporal or spatial sensitivity of one particular technique can be mutually overcome by the others, depending on the pathology of interest. The injection of multimodal contrast agents, which enhance all of the imaging features, could: (i) reduce the scanning time of techniques; and (ii) reduce the dose of chemicals for further safe diagnostics (3). Moreover, it has been shown that multitasking diagnostics that combine techniques such as PET (positron emission tomography) and MRI (magnetic resonance imaging) could be really improved if effective multimodal contrast agents exist (4,5). The fact that PET images provide functional information about the disease with high sensitivity (6) speeds up the development of clinical PET and hybrid PET/computed tomography (CT) cameras. Although PET imaging provides information about physiological and pathophysiological processes, such a technique is limited by the low anatomical resolution (7). On the other hand, MRI offers high-resolution images for anatomical information, especially when a specific contrast agent is injected (8). Indeed the addition of a contrast agent improves the quality of the MRI signal and allows distinguishing different structures that depend principally on tissue density and water content. Paramagnetic gadolinium complexes have been commercialized as powerful contrast agents

* *Correspondence to: F. Lux, ILM, UMR 5306 – Université Claude Bernard Lyon 1, Université de Lyon, 69622 Villeurbanne Cedex, France. Email: francois.lux@univ-lyon1.fr*

a *C. Truillet, J. Brugière, M. Martini, L. Sancey, T. Brichart, F. Lux, O. Tillement*
ILM, UMR 5306 – Université Claude Bernard Lyon 1, Université de Lyon, 69622 Villeurbanne Cedex, France

b *P. Bouziotis, C. Tsoukalas*
Radiochemistry Studies Laboratory, Institute of Nuclear and Radiological Sciences and Technology, Energy and Safety, National Center for Scientific Research 'Demokritos', Athens, Greece

c *F. Denat*
Institut de Chimie Moléculaire de l'Université de Bourgogne, UMR CNRS 6302, Université de Bourgogne, 21078 Dijon Cedex, France

d *F. Boschetti*
CheMatech, 21000 Dijon, France

e *U. Darbost, I. Bonnamour*
ICBMS, UMR 5246 – Université Claude Bernard Lyon 1, Université de Lyon, 69622 Villeurbanne Cedex, France

f *D. Stellas*
Department of Cancer Biology, Biomedical Research Foundation, Academy of Athens, Athens, Greece

g *C. D. Anagnostopoulos*
Center for Experimental surgery, Clinical and Translational Research, Biomedical Research Foundation, Academy of Athens, Athens, Greece

h *V. Koutoulidis, L. A. Moulopoulos*
Department of Radiology, University of Athens Medical School, Areteion Hospital, Athens, Greece

i *P. Perriat*
Matériaux Ingénierie et Science, INSA Lyon, UMR 5510, 69621 Villeurbanne Cedex, France

that are also able to highlight tumour tissue regardless of surrounding healthy zones (9). These positive contrast agents have the advantage of enhancing the local signal, which is more easily detectable than the negative signal produced by negative contrast agents such as iron oxide nanoparticles. The PET technique seems to be an exceptional complement to MRI diagnostics thanks to its metabolic specificity and the ability of tumour differentiation and mapping.

Multimodal nanoparticles have received considerable attention because of their favourable distribution and targeting kinetics, supporting the imaging (10) and even the therapeutic effect (2). On this point, our team has developed a multimodal platform of agents (called AGuIX) constituted of a polysiloxane matrix scaffold that incorporates chelating molecules such as DOTAGA (1,4,7,10-tetraazacyclododecane-1-glutaric anhydride-4,7,10-triacetic acid). Depending on the specific application (diagnostic or therapy), these chelating sites could immobilize a wide variety of contrast agents such as paramagnetic Gd^{3+} ions for MRI and/or ^{111}In for single-photon emission computerized tomography (SPECT) imaging. The AGuIX particles showed promising results in terms of biodistribution and theranostic effects (radiosensitization guided by MRI) (11,12) Although the commonly used radionuclides for PET are mainly ^{18}F (half-life 110 min) and ^{11}C (half-life 20 min), ^{68}Ga is increasingly (half-life 68 minutes) gaining popularity because it can be obtained from a commercially available $^{68}Ge/^{68}Ga$ generator system that delivers the ^{68}Ga nuclide reliably for up to a year, without the need of a cyclotron (13,14). Nevertheless molecules derived from 1,4,7,10-tetraazacyclododecane-1,4,7,10-tetraacetic acid (DOTA), which appear as suitable for Gd^{3+} ions (log β =25.6), show relatively poor affinity for ^{68}Ga (log β =13.7), whereas derived 1,4,7-triazacyclononane-N,N′,N″-triacetic acid (NOTA) chelates (such as NODAGA – 2,2′-(7-(1-carboxy-4-((2,5-dioxopyrrolidin-1-yl)oxy)-4-oxobutyl)-1,4,7-triazonane-1,4-diyl)diacetic acid) offer a strong complexation constant for ^{68}Ga (log β =30.98) (15). In this paper we describe the preparation and characterization of nanoparticle tracers that entrap both DOTAGA and NODAGA complexes for PET and MRI multitasking techniques.

An accurate quantification of available chelating sites per particle is essential for further applications of AGuIX as contrast agents in both PET and MR imaging. We propose two strategies for the estimation of vacant DOTAGA and NODAGA molecules: one strategy based on the absorption titration and the second one based on an innovative luminescence method. Contrary to current titration techniques that allow quantification of only one family of chelating sites, we are able to estimate both the contributions of NODAGA and DOTAGA.

2. MATERIALS AND METHODS

2.1. Chemicals

Sodium hydroxide (NaOH, 99.99%), tetraethyl orthosilicate ($Si(OC_2H_5)_4$, TEOS, 98%), aminopropyl triethoxysilane ($H_2N(CH_2)_3$-$Si(OC_2H_5)_3$, APTES, 99%), triethylamine (TEA, 99.5%) and dimethyl sulphoxide (DMSO, 99.5%) were purchased from Sigma-Aldrich Chemicals. Cy5.5 mono-NHS-ester (CY5.5, 75.4%) was purchased from Amersham Bioscience. Diethylene glycol (DEG, 99%) was purchased from SDS Carlo Erba (France). Diethylene triamine pentaacetic acid (DTPA), DOTAGA and NODAGA were furnished by Chematech (France). Gadolinium chloride hexahydrate ([$GdCl_3$, $6H_2O$], 99%) and gadolinium oxide cores were provided by Nano-H S.A.S. (France). Acetone (reagent grade) was purchased from Sodipro (France) and was used as received. Only Elga Purelab Ultra water was used for the preparation of the aqueous solutions.

2.2. Synthesis of Gadolinium-based Ultrasmall Rigid Platforms

These particles were obtained by a top-down synthesis method. First, gadolinium oxide cores were synthesized in DEG. The oxide core was then coated with a polysiloxane shell induced by hydrolysis-condensation of convenient silane precursors in the presence of gadolinium oxide cores. Afterwards, NODAGA and DOTAGA were covalently grafted on the nanoparticles via an amide bond. All these steps were performed in DEG. The transfer from DEG to water induces core dissolution, leading to a hollow polysiloxane structure. This latter collapses and fragments into small and rigid scaffolds of polysiloxane. The DOTAGA and NODAGA ligands, on the surface of the particles, chelate the dissolved gadolinium cations.

2.2.1. *Gd_2O_3 core synthesis*

The preparation of nanostructured Gd_2O_3 cores follows the well-known polyol method under argon atmosphere. An amount of 55.8 g of [$GdCl_3$, $6H_2O$] was first dissolved in 1L of DEG. The 10 min progressive addition of sodium hydroxide solution (14.85 mL at 10 mM) at 410 K followed by a thermal annealing at 450 K for 5 h allows the formation of monodisperse Gd_2O_3 oxide nanoparticles (1.7 nm (±0.1 nm)). A transparent colloid was obtained and its stability in DEG was ensured for several months.

2.2.2. *Polysiloxane coating of Gd_2O_3 cores*

A polysiloxane shell growth on the oxide cores was induced by hydrolysis-condensation of silane precursors at 310 K. The addition of an APTES and tetraethyl orthosilicate (TEOS) precursors mixture (60:40 molar ratio) in the presence of a basic catalyst solution (DEG with 0.1 mM of TEA and 10 mM of water) induces a progressive polysiloxane coating of the Gd_2O_3 cores. Namely, 2.80 mL of APTES, 1.85 mL of TEOS and 6.80 mL of the catalyst solution were added in the solution containing the nanoparticles at each step. Between single additions, the solution was left under stirring for 12 h. The number of single additions (in this case, 10) determines the thickness of the final polysiloxane coating.

2.2.3. *NODAGA and DOTAGA labelling*

The covalent grafting of NODAGA and DOTAGA molecules onto the Gd_2O_3 core–SiOx shell particles is ensured by an amide bond between the activated NHS groups for the NODAGA and the anhydride function for the DOTAGA and the amino groups relative to APTES molecules. A ratio of 0.2 NODAGA ligands per gadolinium atom was added to the solution. One hour later, two DOTAGA ligands per gadolinium were added to the solution. The NODAGA and DOTAGA ligands provide a large excess of chelators in the solution. The addition of each chelating species is delayed by 1 h. The mixture was stirred for 72 h at room temperature to complete the reaction.

2.2.4. *Purification*

The addition of 3.5 L of acetone leads to the solid-phase precipitation of the colloidal solution. The acetone was then removed by filtration via a sintered glass funnel (16 μm to 40 μm of porosity) and nanoparticles were dispersed in 500 mL water. After the pH adjustment of the solution to 4.5, the colloid was aged for 12 h at 300 K. Further purification steps of functionalized nanoparticles were made by ultrafiltration membranes (Sartorius Stedim Vivaflow® membranes with 5 kDa cut-off threshold) at pH 5. A DTPA solution (at 5 mM) was added to the purified solution. The solution was stirred for 1 h, after which the pH was adjusted to 5.5. The solution was stirred for 12 h at room temperature and then purified by tangential filtration until the desired purification rate of higher than 103 was reached. The largest impurities were removed by 0.2 μm filtering. The sample was then freeze-dried using a Christ Alpha 1-2 lyophilizer for long-term storage.

2.2.5. *^{68}Ga nanoparticle labelling*

For a typical preparation of ^{68}Ga-labelled AGuIX nanoparticles, the AGuIX nanoparticles at 10 mm per gadolinium were mixed with sodium acetate buffer (pH 5.6) and 200 μL of ^{68}Ga eluate (10 MBq per labelling) were consequently added. The mixture was then incubated for 20 min at 40 °C.

2.3. Materials and Instruments

2.3.1. *Dynamic light-scattering measurements*

Direct measurement of the particles-size distribution (i.e. the average size and the mean standard deviation) was performed using a Zetasizer Nano ZS from Malvern Instruments (He–Ne laser 633 nm, 5 mW, with 173° Non-Invasive Back Scatter (NIBS) detector and narrow band filter).

2.3.2. *ζ-Potential measurements*

The ζ-potential of the nanoparticle surface was measured by a Zetasizer Nano ZS from Malvern Instruments. The colloidal solution was first diluted in an aqueous solution containing 0.01 mM of NaCl and then titrated by autotitrator unit MPT2.

2.3.3. *Inductively coupled plasma mass spectrometry analysis*

Determination of the gadolinium content in a sample was performed by inductively coupled plasma mass spectrometry (ICP-MS) analysis. Before measuring gadolinium concentration, samples of colloidal solution were dissolved in concentrated nitric acid for 24 h. The samples were then diluted with water, until the nitric acid concentration in water reached 5%. Chemical analyses were also performed on the as-prepared samples at the 'Service Central d'Analyses du CNRS' (Solaize, France) by ICP-MS, and enabled determination of the C, N and Si contents to a precision of 0.55%.

2.3.4. *Fluorescence measurements*

The time-resolved emission spectra as well as the lifetime decays were collected at room temperature using a Cary Eclipse spectrophotometer developed by Agilent Technologies (75 kW Xenon flash lamp, Czerny-Turner monochromators, Δpulse =2 μs, 800 V PM detector). Samples were diluted in deionized water (nanoparticle concentration equal to 100 μm) to obtain an optical density <0.10 (at the excitation wavelength of 395 nm), in order to prevent reabsorption.

2.3.5. *Relaxometry*

Relaxation time measurements were performed using a Bruker Minispec MQ60 nuclear magnetic resonance analyser, operating under a 1.4 T magnetic field.

2.3.6. *Mass spectrometry*

Full-scan mass experiments were performed using a linear quadrupole ion trap mass spectrometer (LTQ, Thermo Fisher Scientific, San Jose, CA) with enlargement for the high 2000–4000 Th range. The nanoparticle solution was electrosprayed at a flow rate of 20 μL/min in positive ion mode.

2.3.7. *Magnetic Resonance Imaging*

The MRI was performed on a 1.5 T MR unit (Intera; Philips Medical Systems, Best, The Netherlands). Coronal T1-Weighted images (Turbo Spin Echo and 3D Fast Field Echo) with fat saturation were acquired using a surface multichannel coil.

2.3.8. *The PET computed tomography imaging*

Imaging was performed with a clinical PET/computed tomography (CT) system (Biograph 6, Siemens Healthcare, Erlangen, Germany). The CT scans were acquired using a tube voltage of 80 kV, current of 50 mA, slice thickness 1.25 mm, pitch 0.8 and kernel B10s for reconstruction. A high-resolution PET examination was performed using an acquisition time of 40 min/bed position. The PET images were reconstructed using an iterative mode (OSEM Iterative reconstruction algorithm, six iterations and 16 subsets) and a matrix size of 256×256.

2.4. *In vitro* Studies

2.4.1. *Cell lines*

Two line cells were used for evaluating the cytotoxicity of nanoparticles, one from a tumour and the other from healthy cells: U87MG and HEKβ_3. The cell line U87MG is a human primary glioblastoma cell line derived from human malignant gliomas, whereas HEKβ3 is a cell line derived from human embryonic kidney (very easy to transfect), transfected with the integrin subunit Bêta 3.

2.4.1. *Toxicity of AGuIX*

To evaluate the cytotoxicity of the nanoparticles AGuIX, a 3-(4,5-dimethylthiazol-2-yl)-2,5-diphenyltetrazolium bromide (MTT) assay was conducted on the two different cell lines. Cells were plated at a density of 3×10^3 cells per well in 96-well plates and subsequently incubated for 24 h with AGuIX at a wide concentration range: from 0.1 mM per gadolinium to 20 mM per gadolinium. One day after incubation, the cells were washed with a phosphate buffer solution and then Dulbecco's modified Eagle's medium and MTT solutions were added. After incubation for another 6 h, the medium containing MTT was removed and a solubilization solution made of 10% Triton-X 100 in acid isopropanol was added into each well. The plates were gently shaken for 10 min at room temperature. Then, the absorbance

at 570 nm subtracted from 650 nm to act as control was measured. It was possible to determine the cell viability as the ratio of the absorbance of tests cells subtracted from the medium control wells over the absorbance of the untreated wells subtracted from the medium control wells.

2.5. *In Vivo* Studies

The *in vivo* behaviour of the radiolabelled compound was initially evaluated in normal Swiss mice. Intravenous administration was performed at 20 kBq/100 µL per mouse, via the tail vein. The *ex vivo* biodistribution study was performed at 30, 60 and 120 min post-injection. All animal experiments were performed in compliance with EC Directive 86/609 and its implementation in national legislation (updated version EL 56/2013).

3. RESULTS

3.1. Synthesis and Purification

The synthesis of AGuIX contrast agents follows an original top-down method used for the DOTAGA-based particles reported elsewhere (11,12). Briefly, a gadolinium oxide core of 1.7 nm is obtained by addition of caustic soda on gadolinium trichloride previously dissolved in diethylene glycol (DEG). Gadolinium oxide cores are then coated with a polysiloxane shell after addition of APTES and TEOS precursors (16), and NODAGA (0.2 per gadolinium atom) and DOTAGA (two per gadolinium atom) were grafted on the amine functions of the core–shell particles. The NODAGA ligands were chosen because of their high affinity with $^{68}Ga^{3+}$, whereas the DOTAGA ligands were specifically selected for their efficient chelation of Gd^{3+} ions (17–19). Moreover, thanks to their carboxylic acid groups, they make the core–shell particles hydrophilic, conferring to them good colloidal stability in biological buffers. The particles were then transferred in water and purified. At that moment, the oxide core was dissolved and the DOTAGA and the NODAGA moieties chelated the gadolinium ions that were issued from the dissolution of the oxide core (see Scheme 1) (11,12).

The further addition of DTPA ligands induces the transmetallation of gadolinium ions from the NODAGA to the DTPA, making the NODAGA ligands free to be radiolabelled. The phenomenon is directly due to the higher complexation constant towards gadolinium of DTPA compared with that of NODAGA (log β =22.5 for DTPA vs 13.7 for the NODA) and to the slow kinetics of demetallation for the DOTAGA (20). The final solution was purified by ultrafiltration with 5 kDa cut-off polyethersulphone membrane for the total elimination of residual DTPA and DTPA[Gd^{3+}] (see Scheme 1).

The final colloidal solution has been characterized by dynamic light scattering and a hydrodynamic diameter equal to 2.5 nm (±0.1 nm) has been found (see Scheme 1d). Moreover, potential assays confirm a slight positive charge of +4.5 mV at physiological pH (see Supporting Information). Finally, the particles were freeze-dried for storage and are stable for months.

3.2. Mass of AGuIX obtained by MS

Mass spectroscopy allows the calculation of the average composition of AGuIX nanoparticles. The nanoparticles were subjected

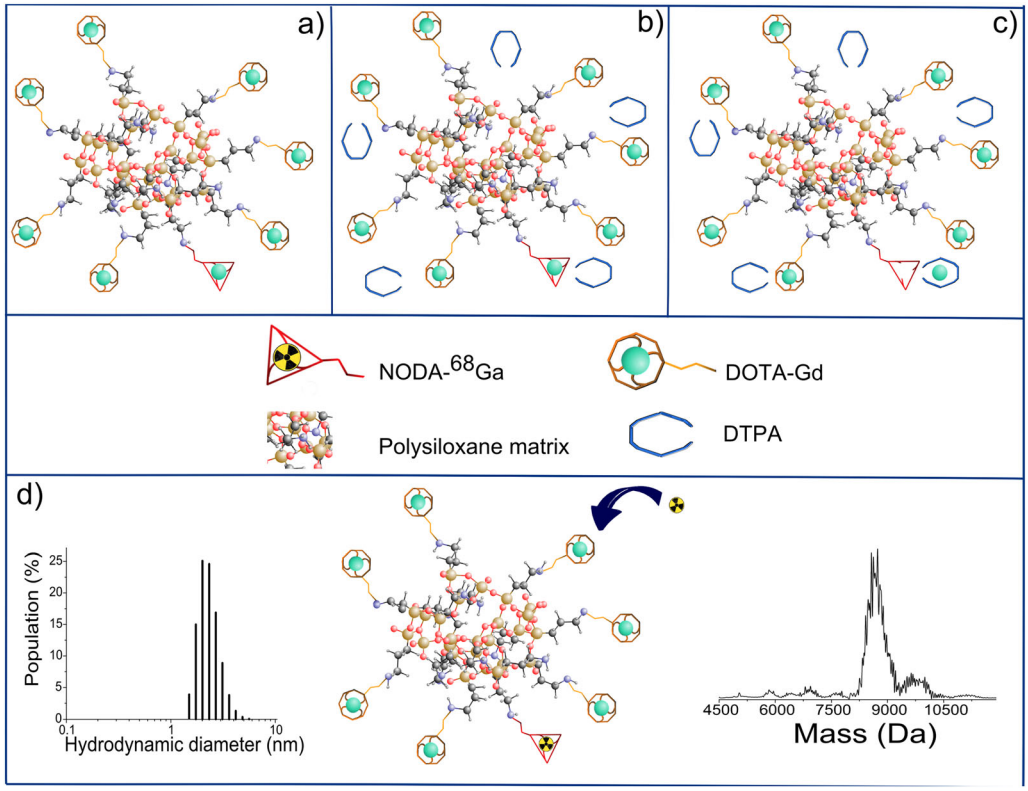

Scheme 1. Final steps in the synthesis of AGuIX nanoparticles: (a) nanoparticles after transfer in water; (b) addition of DTPA ligands; (c) chelation of Gd^{3+} previously trapped in NODAGA ligands; (d) possibility of radiolabelling with ^{68}Ga on accessible NODAGA ligands. On the left, the dynamic light scattering distribution of AGuIX and on the right their mass distribution determined by deconvolution with a multiplicative correlation algorithm.

Table 1. Relaxivities comparison between AGuIX® and clinical product DOTAREM® at 60 MHz

Relaxivity	AGuIX® ($mM^{-1}.s^{-1}$)	DOTAREM® ($mM^{-1}s^{-1}$)
r_1	10.3	3.4
r_2	13.4	4.8

to electrospray ionization (ESI) that generates gas-phase ions that provide mass-to-charge information. The results obtained have been exploited because the 'envelope' of peaks was stable and the relative abundance of the different peaks was found to be dependent only on the ESI/MS experimental conditions. A multiplicative correlation algorithm (MCA) was then used to estimate the mass of the nanoparticles (see Scheme 1d (inset), the mass distribution generated).

The results reveal an average mass value of 8.7 ± 0.2 kDa per particle in coherence with the dynamic light-scattering measurements. The fragmentation mass spectrometry analysis also confirmed the presence of free NODAGA and DOTAGA[Gd^{3+}] upon the nanoparticles (see Supporting Information). Some fragments in the positive mode of the ESI spectrum directly highlight the covalent conjugation of the NODAGA to the APTES of the polysiloxane matrix via the primary amine side-chain group. In the low *m/z* range of the MS spectrum in positive mode (between *m/z* 250 and *m/z* 2000), the *m/z* 461 peak was found to be characteristic of NODAGA-functionalized AGuIX (Supporting Information – Figure SI 3). Some specific fragments of DOTAGA issued from the AGuIX have been observed, such as the m/z 720 peak that is specific to the $[Si(OH)^{3-}$ DOTA[Gd^{3+}]]$^{-}$ (Supporting Information – Figure SI 3).

3.3. Relaxivity Studies

The efficiency of AGuIX particles as a MRI contrast agent was evaluated by the measurements of the longitudinal and the transversal relaxivity (respectively r_1 and r_2). One of the common approaches to increase relaxivity is to slow down the molecular tumbling by attaching gadolinium complexes to a macromolecule through rigid linkages (21,22). Longitudinal and transversal relaxivities are reported in Table 1 and have been compared with a commercial contrast agent called DOTAREM®.

Relaxivity measurements gave a longitudinal relaxivity r_1 of 10.3 $mM^{-1}s^{-1}$ per gadolinium at 60 MHz, almost three times superior to the clinically used gadolinium agent DOTAREM and a low r_2/r_1 ratio of 1.3 in agreement with values of the literature for T_1 contrast agents.

3.4. Quantification of Available Chelate Sites for Radiolabelling

3.4.1. *Absorbance assays*

The most popular and intuitive technique for the quantification of binding sites is represented by the absorption titration. The Lambert Beer's law states that the absorbance is directly proportional to the concentration of species in the sample, each one weighted by the molar extinction coefficient ε. The Cu^{2+} ions are added as tracers for absorption titration because their complexation with DOTA and NODA molecules causes an intense signal in the visible region that is specific of chelating molecules (23,24). The signal collected is then the sum of the AGuIX nanoparticle, DOTAGA[Cu^{2+}], NODAGA[Cu^{2+}] and [Cu^{2+}] ions contributions (eqn (1)):

$$\begin{aligned} A(\lambda) &= \Sigma_i A_i\left(\varepsilon_{\lambda,i}, l, c_i\right) \\ &= \varepsilon_{\lambda,DOTA[Cu]} c_{DOTA[Cu]} l + \varepsilon_{\lambda,NODA[Cu]} c_{NODA[Cu]} l \\ &\quad + \varepsilon_{\lambda,AGuIX} c_{AGuIX} l + \varepsilon_{\lambda,Cu} c_{Cu} l \end{aligned} \quad (1)$$

The molar extinction coefficients have been determined from standard references. The mathematical deconvolution of the absorbance curve provides the base vector for each species in the solution and then the number of available sites for complexation.

Figure 1 summarizes the absorption curves of reference solutions with their maximum centred at 741 nm for DOTAGA [Cu^{2+}], at 672 nm for NODAGA[Cu^{2+}] and at 820 nm for free [Cu^{2+}] ions. The AGuIX nanoparticles show a continuous exponential decrease till the red-edge wavelengths. For the titration we chose the range of wavelengths between 450 nm and 575 nm, where only AGuIX, DOTAGA[Cu^{2+}] and NODAGA[Cu^{2+}] absorb.

The progressive addition of Cu^{2+} ions (i) increases the absorption peak and (ii) red-shifts the maximum from 720 nm to 770 nm for concentrations higher than 8% (0.5 mm) (Fig. 1b). The unmodified peak position for low concentrations of Cu^{2+} ions is due to the progressive complexation of metal ions by the chelating agents at the nanoparticle surface, whereas the absorbance maximum shift (for concentrations higher than 8%) depends on the presence of free Cu^{2+} ions in solution. Considering the critical concentration of 8%, which corresponds to the

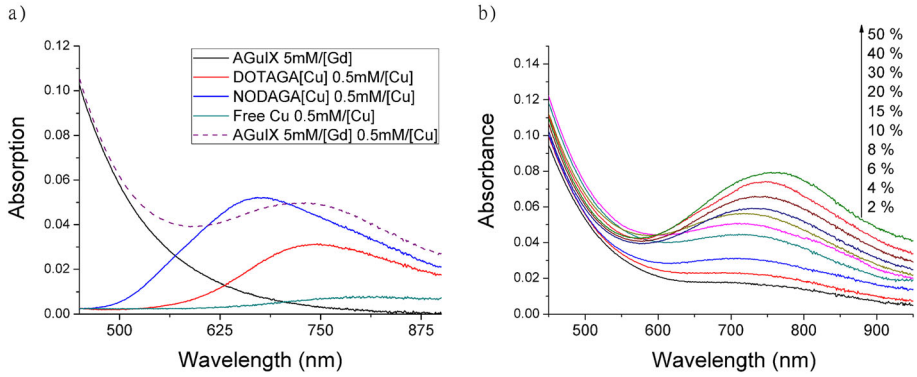

Figure 1. (a) Absorption spectra with different standard solutions (DOTAGA[Cu^{2+}], NODAGA[Cu^{2+}] and Cu^{2+}) for a concentration of 1 mM of copper at pH 3. (b) Absorption spectra of the nanoparticles AGuIX as a function of the copper per gadolinium atom (in %).

maximum number of available sites for Cu^{2+} chelation, the estimation of available NODAGA and NODAGA ligands is equal to 6.5% (0.325 mm) and 1.5% (0.075 mm) respectively.

3.4.2. *Luminescence assays*

The quantification of available chelating sites by absorbance titration is undoubtedly critical, because of the close overlap between each contribution (NODAGA, DOTAGA and the AGuIX). Faced with such systematic error, luminescence titration seems to be the best way to bypass the resolution limits of the absorption technique. The concept of this innovative tool for accurate chelates quantification arises from (i) the specific signature of lanthanide luminescent centres with the chelating agent, (ii) the high sensitivity at low sample concentrations and (iii) the exclusion of parasitic signals due to the environmental background. As seen for the case of absorbance titration, the fluorescence signal also can be a linear combination of single contributions only for highly diluted samples.

Although the fluorescence signal is usually not proportional to the emitter concentration because of the inner filter effect, at very high dilutions the deviation from linearity is acceptable (25).

Based on these considerations, the fluorescent signal is then the sum of three components due to the environment of the tracer (in this case Eu^{3+} ions have been preferred to the Cu^{2+} for their specific luminescence signature): DOTAGA[Eu^{3+}], NODAGA[Eu^{3+}] and free [Eu^{3+}] (eqn (2)):

$$I = K_{DOTA[Eu]} \cdot c_{DOTA[Eu]} + K_{NODA[Eu]} \cdot c_{NODA[Eu]} + K_{Eu^{3+}} c_{Eu^{3+}} \quad (2)$$

Indeed, the europium ion was chosen because of (i) its chemical reactivity very close to the gadolinium ions, (ii) the stability constants for chelation (DOTAGA, NODAGA) are similar to gadolinium, (iii) the luminescence spectrum that is really sensitive to the ion environment helps the separation of each component and (iv) the long lifetime allows time-resolved assays that bypass the fluorescence background of residual organic impurities. Once the *K* constants have been estimated by standard reference assays (See Supporting Information), the mathematical iteration of luminescence curve fittings provide the number of available sites for complexation.

Focusing only on the magnetic dipole of europium (595 nm), an excellent linearity of emission signal with the concentration in the range of 0.1–2.5 mM was evident. The *K* factors of eqn (2) were then easily estimated: I_{595nm} =273.04; $C_{DOTAGA[Eu3+]}$ =136.25 and $C_{NODAGA[Eu3+]}$ =18.13 C_{Eu3+}. The progressive addition of europium tracers from 1% (0.025 mM) up to 50 % (1.25 mM) reveals a change in fluorescence intensity increase around 8% (Fig. 2). In the first portion of the curve (Eu^{3+} amounts <8% per gadolinium), the intensity measured increased dramatically with the amount of tracers added due to the complete chelation of Eu^{3+} ions by both DOTAGA and NODAGA molecules. The subsequent change in slope for higher concentrations proves the presence of additional free europium ions in the solution. From the fluorescence titration, the 8% threshold obtained was directly correlated to the number of available complexation sites upon AGuIX nanoparticles and the value confirms previous absorption titration results.

3.4.3. *Lifetime titration assays*

A third method for the quantification of chelates is based on the lifetime of titration. The fact that europium ions display a long lifetime and the intensity decay rates is independent of sample concentration seems to be interesting for the evaluation of the number of binding sites. The luminescence process, as a spontaneous phenomenon, is simply described by the equation:

$$I(t) = I_0 e^{-t/\tau} \quad (3)$$

where I_0 represents the intensity immediately following the excitation pulse and τ is the time spent by the tracer at the excited state before its relaxation decay (26). The linear combination previously mentioned for both absorption and luminescence titration also can be used for lifetimes. Considering a specific lifetime value τ_i for each environment of tracer used, we obtained:

$$I(t) = \sum_i \alpha_i \exp(-t/\tau_i) \quad (4)$$

The fitting of decay curves allows the estimation of pre-exponential factors α_i that are proportional to the percentage of each species. The further integral calculus of decay curves leads to the intensity contribution of each species I_i (termed decay-associated spectra, DAS) and finally to the relative concentrations [c_i] in the sample:

$$I_i(\lambda) = f_i \times I(\lambda) \quad (5)$$

with

$$f_i = \frac{\alpha_i \tau_i}{\sum_j \alpha_j \tau_j} \quad (6)$$

The coefficient *f* is defined as the fractional contribution of the component. The concentration of each component is then directly proportional to f_i

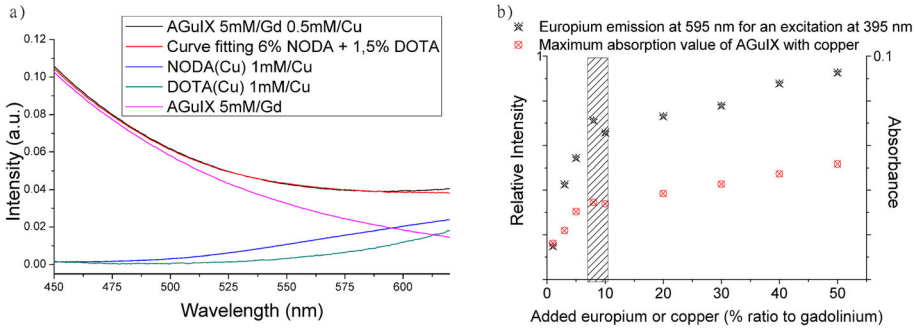

Figure 2. (a) Comparison of the absorption experimental curve of nanoparticles with copper, with the fitting curve obtained thanks to the calibration curve of NODAGA[Cu^{2+}] and DOTAGA[Cu^{2+}] and the nanoparticles alone. (b) Titration of available chelating sites by europium emission and copper absorption.

$$\%[Ci] \propto \frac{f_i . \Sigma \alpha_i}{\alpha_i} \quad (7)$$

with $\frac{\alpha_i}{\sum_i \alpha_i}$ the normalized factor.

Reference assays showed specific lifetime values that depend on the chelating molecule: τ_{DOTAGA} =625 ms, τ_{NODAGA} =390 ms and τ_{free} =120 ms. The decrease in the lifetime is directly correlated to the higher number of water molecules coordinated to europium. The mathematical iteration of curve fitting allows estimation of the coefficients (α_i,τ_i) and then, following the formula mentioned above, the fractional contributions f_i. As seen in previous titration techniques, the concentration of 8% separates the samples where complete chelation has occurred and the samples that also present free tracers (Fig. 3). Moreover, the fractional intensities show the major contribution of NODAGA[Eu^{3+}] instead of DOTAGA[Eu^{3+}] and confirm that AGuIX® particles contain 6.5% of available NODAGA sites and only 1.5% of DOTAGA.

3.5. Determination of the AGuIX Molecular Structure

Taking into account the information provided by MS, elemental analysis and optical titration we were able to suggest the probable average composition of the AGuIX tracers. Indeed, the optical assays coupled with the information obtained by elemental analysis (absolute error ranging below 0.5% of the weight percentages) produce the ratio: Gd_1:$APTES_{2.43}$:$TEOS_{2.31}$:$DOTAGA_{1.015}$:$NODAGA_{0.065}$. On the other hand, considering the global mass of about 8.7 ± 0.2 kDa, we can propose the following average composition $Gd_{8.2}$:$APTES_{20.0}$:$TEOS_{19.0}$:$DOTAGA_{8.3}$:$NODAGA_{0.5}$ for one individual AGuIX, which is in total agreement with the composition produced by ICP-MS (Table 2).

3.6. Evaluation of AGuIX Labelling Potential and Stability

Radiochemical purity after ^{68}Ga labelling was determined by ITLC (instant thin-layer chromatography), using KCL 0.2 M as the mobile phase (Fig. 4c). *In vitro* stability of ^{68}Ga-AGuIX was assessed in saline and serum for up to 3 h. For the serum stability studies, 50 µL ^{68}Ga-AGuIX® conjugate was added to 450 µL serum, and the mixture was incubated at 37 °C. Samples were taken at 10, 60 and 180 min and assessed by ITLC silica gel, with 0.2 M KCl (pH 3) as the mobile phase.

As reported in Fig. 4c, the AGuIX nanoparticles were successfully labelled with ^{68}Ga with high radiochemical purity

Table 2. Chemical composition of the nanoparticles deduced from ICP-MS

	Element mass fraction (%)			
	Gd	Si	N	C
Elementary analysis	12.42	10.48	7.39	24.34
Calculated	12.71	10.72	7.48	25.49

a)

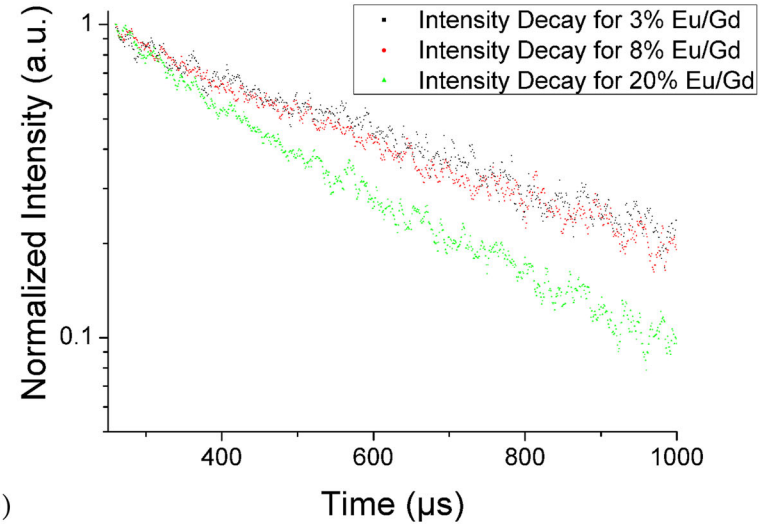

b)

% Europium/ Gadolinium	Pre exponential factors			Fractional intensity			Deduced concentration ratio / Gd amount		
	α1	**α2**	**α3**	**f1**	**f2**	**f3**	**%[C1]**	**%[C2]**	**%[C3]**
3	-	0.08	0.22	-	0.18	0.82	-	1.52	1.48
8	-	1.57	0.18	-	0.82	0.083	-	6.55	1.45
20	0.3721	0.1	0.015	0.48	0.4	0.11	12.02	6.54	1.44

Figure 3. (a) Luminescence decay of the solution with different percentages of europium per gadolinium. A multiplicative correlation algorithm fits the experimental curve according to the equation $I(t) = \Sigma i\ \alpha_i \exp(-t/\tau_i)$. (b) Recapitulative table with different parameters in order to analyse the decay curve. The lifetime of each compound was determined as: 1 = [Eu^{3+}], 2 = NODAGA[Eu^{3+}] and 3 = DOTAGA[Eu^{3+}].

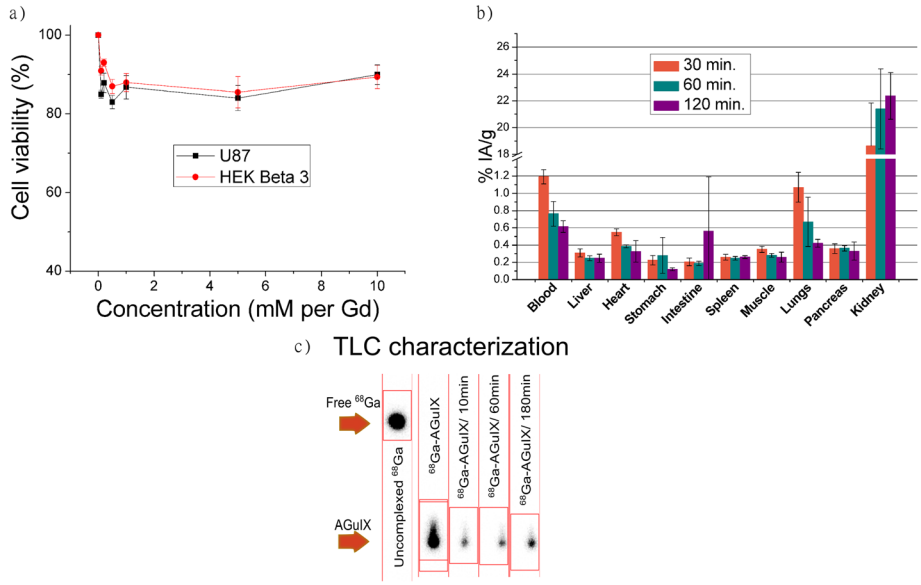

Figure 4. (a) Evaluation of the toxicity of the nanoparticle AGuIX by MTT assay on two different cell lines (U87 and HEKβ3). (b) Biodistribution study performed at 30, 60 and 120 min post injection on healthy mouse. (c) Stability studies in serum of the nanoparticles at different ageing times. The concentration of the nanoparticles is 10 mM per gadolinium.

(>97%). The ^{68}Ga-AGuIX nanoparticles were stable at retention times up to 3 h.

3.7. Toxicity of the Nanoparticles

Nanoparticle toxicity was investigated on two cell lines, one tumour cell line (U87) and one normal cell line (HEKβ_3; Fig. 4). The MTT assay was used to evaluate the toxicity of the nanoparticles without labelling and indicated that the AGuIX nanoparticles displayed at least 80% cell viability for both cell lines, even at the highest feed concentration.

On healthy cells and on tumour cells, the nanoparticles do not show any toxicity. The absence of unchelated Gd^{3+} was confirmed by titrations with xylenol orange, which is an indicator specific for complexometric metal titrations. Thanks to the low complexation constant of Gd^{3+} by xylenol orange (log K =5.8), there is no risk of extracting any Gd^{3+} from highly stable complexes such as DOTAGA[Gd^{3+}].

3.8. Dynamic Distribution of AGuIX in Normal Nude Mice

Healthy nude mice (n = 3) were used to investigate the biodistribution of the probes *in vivo*. After injection, no animals showed any symptom such as pain, illness or abnormal

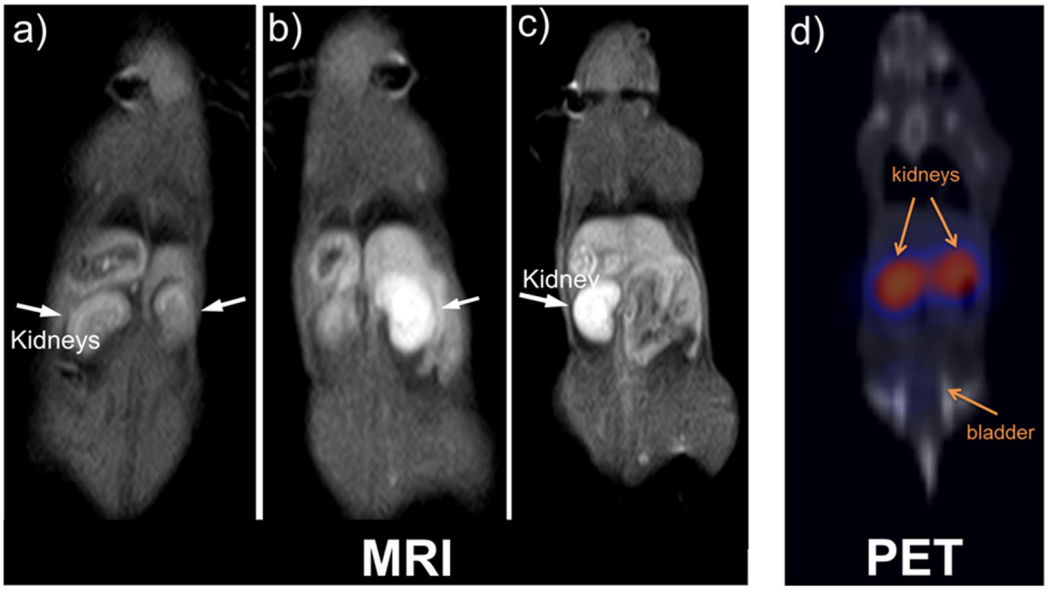

Figure 5. The MRI/PET images on the same mouse with AGuIX. (a–c) The MR images of a male mouse that was injected with 20 μmol labelled AGuIX solution, 60 min prior to the MRI examination. We note a definite enhancement of the kidneys (arrows in b and c). Compare with corresponding slices of the kidneys (arrows in a) of a non-injected male mouse, acquired with the same imaging parameters. (d) A PET/CT image with 0.925 MBq of 68Ga-AGuIX (injected volume: 150 μl) and placed on a warm polystyrene pad for 30 min.

behaviour. After the PET/MRI experiment, the animals were euthanized and then the major organs were isolated (the *ex vivo* measurements are summarized in the Fig. 4b). Biodistribution studies in normal Swiss mice showed that ^{68}Ga-AGuIX cleared rapidly from the blood via the kidneys to the urine, resulting in extremely low background activity in all other analysed tissues (<2% injected dose (ID)/g at 120 min intraperitoneally (p.i.)).

3.9. The PET/MRI of ^{68}Ga-AGuIX

The PET images and MRI images (Fig. 5) were successfully gathered after nanoparticle injection. Mice were anaesthetized with an intraperitoneal injection of a mixture of ketamine (100 mg/kg) and xylazine (15 mg/kg). They then received by retro-orbital injection 0.925 MBq of ^{68}Ga-AGuIX (injected volume: 150 µl) and were placed on a warm polystyrene pad for 2 h. The PET CT examination was then performed using a clinical PET/CT system. The MR imaging of the same male mouse was performed on a 1.5 T unit, 60 min post-injection of 20 µmol AGuIX®.

The MR images of treated mice exhibited significant contrast enhancement compared with the untreated mice. As the mice were healthy, the nanoparticles were excreted quickly by the kidneys, as previously shown in classic AGuIX nanoparticles assays (11,12). This way of elimination induces a significant contrast enhancement due to the presence of the particles in the kidneys and in the urinary bladder.

On PET/CT images, radioactivity due to AGuIX was observed in the bladder and the kidneys. Any trace of radioactivity in critical organs such as liver, lungs and bone was detected, and this confirms that MRI and PET/CT interpretations were totally coherent in the two imaging techniques.

4. DISCUSSION

Due to the synthesis process of the nanoparticles, all the ligands chelate a gadolinium after the passage of the nanoparticle from the DEG to the water. The addition of DTPA presenting a complexation constant towards gadolinium between DOTAGA and NODAGA permits the specific demetallation of NODAGA during the purification process. To validate this strategy, an accurate quantification of available chelating sites per particle is essential. We propose two strategies for the estimation of vacant DOTAGA and NODAGA molecules: one strategy based on absorption titration and the second one based on innovative luminescence methods. Contrary to current titration techniques that allow quantification of only one family of chelating sites, we were able to estimate both contributions of NODAGA and DOTAGA.

The most popular and intuitive technique for the quantification of binding sites is performed by absorption titration. Absorption assays, thanks to the Lambert Beer's law, provide a signal that is directly proportional to the concentration of species in the sample. The addition of Cu^{2+} ions – that immobilize spontaneously within chelates – shifts the absorption peak as a function of its binding site. The different absorption features allow the quantification of available chelating sites in the sample. The titration was managed by progressive addition of copper with different ratios of Cu^{2+}/Gd from 1% to 50%. As shown in Fig. 2(b), the maximum absorption value of the copper increases drastically from 1% to 8% and shows a clear break in slope after 8%. The steep slope before 8% is due to the progressive complexation of metal ions by the available chelating sites at the nanoparticle surface. Beyond this value, the further addition of Cu^{2+} ions has only a smaller impact on the total absorption because they remain free in solution.

The absorption titration method displays some limits due to the overlap between the characteristic peaks of both NODAGA and DOTAGA molecules in the visible range. Moreover the presence of free Cu^{2+} ions that contribute as chelating molecules decreases the accuracy of quantification of available sites (Fig. 2a). Luminescence titration seems to be the best way to bypass the resolution limits of the absorption technique. As seen for the absorbance titration, the total fluorescence signal is the linear combination of single contributions due to species diluted in the sample (see Supplementary Information). In this case, Cu^{2+} ions have been replaced by Eu^{3+} ions, because they appear as the best luminescent species for this titration (27). The long lifetime of europium ions allows time-resolved assays that bypass the fluorescence background of residual organic impurities in the sample. Luminescence spectra reveal a strong dependence of $^5D_0$–$^7F_1$ (peak centered at 592 nm) transition peak intensities from the environment of europium ions (see Supporting Information). The progressive addition of the europium amount from 1% to 50% reveals a break in fluorescence intensity ($^5D_0$–$^7F_1$ transition) increase around 8%. In the first portion of the curve (Eu^{3+} amounts <8% per gadolinium), the intensity of the 595 nm peak increases dramatically with the amount of Eu^{3+} due to the complete chelation of Eu^{3+} by both DOTAGA and NODAGA molecules. The subsequent decrease in slope with drop in intensity shows the presence of free europium ions in the solution (due to the quenching of fluorescence by water for free europium). The 8% threshold is directly correlated to the number of available complexation sites upon AGuIX nanoparticles, in agreement with the absorption titration result.

We demonstrated that further lifetime titration assays could be adequate to quantify the number of available chelating molecules. The mathematical iteration fitting of decay curves (excitation wavelength at 395 nm and emission wavelength at 595 nm) allows the estimation of the coefficients ($\alpha_i\tau_i$) and hence the fractional contributions f_i for each i species. The lifetime value of europium dramatically depends on the presence of the specific chelating molecule. The critical point of 8% separates the condition for a complete chelation of europium and the presence of free europium ions in solution. Fractional intensities show the major contribution of NODAGA[Eu^{3+}] (6.5%) instead of the small amount of DOTAGA[Eu^{3+}] (1.5%).

Taking into account this number of free chelates and the global mass of about 8.7 kDa and the elemental analysis, the average composition for one individual AGuIX is about $Gd_{8.2}$:$APTES_{20.0}$:$TEOS_{19.0}$:$DOTAGA_{8.3}$:$NODAGA_{0.5}$.

The presence of gadolinium ions on the nanoparticles allows their monitoring by T_1-weighted MRI. Relaxivity measurements gave a longitudinal relaxivity r_1 of 10.3 $mM^{-1}s^{-1}$ per gadolinium ions at 60 MHz, more than two times higher than that of the commercial agent DOTAREM® (3.4 $mM^{-1}s^{-1}$) and a r_2/r_1 ratio of 1.3. The low r_2/r_1 ratio proves that the AGuIX can be an efficient T_1 contrast agent (28). Further labelling with the positron-emitter ^{68}Ga via the remaining available chelates on the nanoparticle surface was accomplished in sodium acetate buffer (concentration of nanoparticles: 25 mM/50 MBq ^{68}Ga). Evaluation of chromatographic profiles showed the correct partition of patterns: the presence of a single spot shifted from the ^{68}Ga reference proved the complete labelling of ^{68}Ga on nanoparticles. Moreover, the deviation from linearity for each chromatographic system was not significant. Accuracy assessments, which showed percentages

of radioactivity recovery over 97%, assured no further post-purification steps were necessary. The nanoparticles are cleared rapidly from the blood to the urine via the kidneys, as established by the biodistribution analysis, due to the small size and the biodegradable properties of AGuIX (29,30). An extremely low residual activity in all untargeted tissues, especially in the critical organs such as the liver and lungs (<2% ID/g at 120 min p.i.) and the long-term stability of ^{68}Ga-AGuIX, as well the high value of longitudinal relaxivity, demonstrate the capabilities for a dual-modality PET/MRI imaging system (31).

The PET/MRI imaging assays were managed on the same healthy male Swiss mice, The MR imaging being performed on a 1.5 T unit, 60 min after the injection, and the PET assays completing the evaluation of the AGuIX contrast agent 60 min after the MR imaging, using a clinical PET/CT system (32).

5. CONCLUSION

Our results emphasize that the ^{68}Ga-AGuIX tracer is a promising tool to simultaneously perform PET and MR imaging. The functionalization of AGuIX by DOTAGA and NODAGA chelates leads to a specific ligand for each imaging functionality (chelation of Gd^{3+} on DOTAGA and $^{68}Ga^{3+}$ on NODAGA). The elimination of these nanoparticles by the kidneys has been confirmed by the two imaging techniques, in good agreement with other studies performed on under 5 nm nanoparticles (32) or dendrimers (33,34). It is explained by the fast clearance through the glomerulus and by consequence, non-specific re-uptake in the proximal tubuli (35). In summary, these nanoprobes would be available for a combined PET/MRI instrument.

Acknowledgements

We wish to thank the COST action TD1004 'theranostics imaging and therapy: an action to develop novel nanosized systems for imaging-guided drug delivery'. Thanks are also due to French program ANR-12-RPIB-0010 Multimage. The authors gratefully acknowledge Professors H.R. Maecke and F. Roesch for provision of the Ga-68 generators used in this study, Dr T. Tsotakos for radiopharmaceutical expertise, and Mr S. Xanthopoulos for technical assistance. The authors acknowledge Dr P. Dugourd and Dr R. Antoine for mass measurements.

REFERENCES

1. Pagel MD. The hope and hype of multimodality imaging contrast agents. Nanomedicine 2011; 6: 945–948; doi: 10.2217/NNM.11.63
2. Lee DE, Koo H, Sun IC, Ryu JH, Kim K, Kwon IC. Multifunctional nanoparticles for multimodal imaging and theragnosis. Chem Soc Rev 2012; 41: 2656–2672; doi: 10.1039/c2cs15261d
3. Willmann JK, van Bruggen N, Dinkelborg LM, Gambhir SS. Molecular imaging in drug development. Nat Rev Drug Discov 2008; 7: 591–560; doi: 10.1038/nrd2290
4. Townsend DW. Multimodality imaging of structure and function. Phys Med Biol 2008; 53: R1–R39; doi: 10.1088/0031-9155/53/4/R01
5. Jennings LE, Long NJ. Two is better than one'-probes for dual modality molecular imaging. Chem Commun 2009; 24: 3511–3524; doi: 10.1039/b821903f
6. Debergh I, Vanhove C, Ceelen W. Innovation in cancer imaging. Eur Surg Res 2012; 48: 121–130; doi: 10.1159/000338193
7. Pauleit D, Stoffels G, Bachofner A, Floeth FW, Sabel M, Herzog H, Tellmann L, Jansen P, Reifenberger G, Hamacher K, Coenen HH, Langen KJ. Comparison of 18 F-FET and 18 F-FDG PET in brain tumors. Nucl Med Biol 2009; 36: 779–787; doi: 10.1016/j.nucmedbio.2009.05.005
8. Louie A. Multimodality imaging probes: design and challenges. Chem Rev 2010; 110: 3146–3195; doi 10.1021/cr9003538
9. Iwaki S, Hanaoka K, Piao W, Komatsu T, Ueno T, Terai T, Nagano T. Development of hypoxia-sensitive Gd^{3+}-based MRI contrast agents. Bioorg Med Chem Lett 2012; 22: 2798–2802; doi: 10.1016/j.bmcl.2012.02.071
10. Brigger I, Dubernet C, Couvreur P. Nanoparticles in cancer therapy and diagnosis. Adv Drug Deliv Rev 2002; 54: 631–651; doi: 10.1016/S0169-409X(02)00044-3
11. Lux F, Mignot A, Mowat P, Louis C, Dufort S, Bernhard C, Denat F, Boschetti F, Brunet C, Antoine R, Dugourd P, Laurent S, Vander Elst L, Muller R, Sancey L, Josserand V, Coll JL, Stupar V, Barbier E, Rémy C, Broisat A, Ghezzi C, Le Duc G, Roux S, Perriat P, Tillement O. Ultrasmall rigid particles as multimodal probes for medical applications. Angew Chem Int Ed 2011; 50: 12299–12303; doi: 10.1002/anie.201104104
12. Mignot A, Truillet C, Lux F, Sancey L, Louis C, Denat F, Boschetti F, Bocher L, Gloter A, Stephan O, Antoine R, Dugourd P, Luneau D, Novitchi G, Figueiredo LC, de Morais PC, Bonneviot L, Albela B, Ribot F, Van Lokeren L, Dechamps-Olivier I, Chuburu F, Lemercier G, Villiers C, Marche P, Le Duc G, Roux S, Tillement O, Perriat P. A top-down synthesis route to ultrasmall multifunctional gd-based silica nanoparticles for theranostic applications. Chem Eur J 2013; 19: 6122–6136; doi: 10.1002/chem.201203003
13. Couturier O, Lacoeuille F, Lefebvre C, Hindre F, Vervueren L, Bouchet F, Le Jeune JJ, Hustinx R. Phenotypic imaging and gallium-68 radiolabeled peptides: Beyond the somatostatin analogs. Méd Nucl 2010; 34: 421–422; doi: 10.1016/j.mednuc.2010.06.020
14. Baum RP, Prasad V, Hommann M, Hörsch D. Receptor PET/CT imaging of neuroendocrine tumors. Recent Results Cancer Res 2008; 170: 225–242.
15. Bartholomä MD, Louie AS, Valliant JF, Zubieta J. Technetium and gallium derived radiopharmaceuticals: comparing and contrasting the chemistry of two important radiometals for the molecular imaging era. Chem Rev 2010; 110: 2903–2920; doi: 10.1021/cr1000755
16. Bridot JL, Faure AC, Laurent S, Rivière C, Billotey C, Hiba B, Janier M, Josserand V, Coll JL, Vander Elst L, Muller R, Roux S, Perriat P, Tillement O. Hybrid gadolinium oxide nanoparticles: multimodal contrast agents for in vivo imaging. J Am Chem Soc 2007; 129: 5076–5084; doi: 10.1021/ja068356j
17. Berry DJ, Ma YM, Ballinger JR, Tavare R, Koers A, Sunassee K, Zhou T, Nawaz S, Mullen GED, Hider RC, Blower PJ. Efficient bifunctional gallium-68 chelators for positron emission tomography: tris (hydroxypyridinone) ligands. Chem Commun 2011; 47: 7068–7070; doi: 10.1039/c1cc12123e
18. Majkowska-Pilip A, Bilewicz A. Macrocyclic complexes of scandium radionuclides as precursors for diagnostic and therapeutic radiopharmaceuticals. J Inorg Biochem 2011; 105: 313–320; doi: 10.1016/j.jinorgbio.2010.11.003
19. Othman M, Desmaële D, Couvreur P, Vander Elst L, Laurent S, Muller RN, Bourgaux C, Morvan E, Pouget T, Lepêtre-Mouelhi S, Durand P, Gref R. Synthesis and physicochemical chararacterization of new squalenoyl amphiphilic gadolinium complexes as nanoparticle contrast agents. Org Biomol Chem 2011; 9: 4367–4386; doi: 10.1039/c1ob00015b
20. Moeller T, Thompson LC. Observations on the rare earths – LXXV(1): The stabilities of diethylenetriaminepentaacetic acid chelates. J Inorg Nucl Chem 1962; 24: 499–510; doi: 10.1016/0022-1902(62)80236-X
21. Prasuhn DE, Yeh RM, Obenaus A, Manchester M, Finn MG. Viral MRI contrast agents: coordination of Gd by native virions and attachement of Gd complexes by azide-alkyne cycloaddition. Chem Commun 2007; 12: 1269–1271; doi: 10.1039/b615084e
22. Trivedi ER, Ma Z, Waters AE, Macrenaris WK, Subramanian R, Barrett GMA, Meade JT, Hoffman MB. Synthesis and characterization of porphyrazine-Gd(III) MRI contrast agent and in vivo imaging of breast cancer xenograft model. Contrast Media Mol Imaging 2014; 9: 313–322; doi: 10.1002/cmmi.1577
23. Delgado R, Sun Y, Motekaitis RJ, Martell AE. Stabilities of divalent and trivalent metal ion complexes of macrocyclic triazatriacetic acids. Inorg Chem 1993; 32: 3320–3326; doi: 10.1021/ic00067a022
24. Brady ED, Chong HS, Milenic DE, Brechbiel MW. Development of a spectroscopic assay for bifunctional ligand-protein conjugates based on copper. Nucl Med Biol 2004; 6: 795–802; doi: 10.1016/j.nucmedbio.2004.04.004
25. Valeur B. Molecular Fluorescence Principles and Applications, 2nd edn. Wiley-VCH: Weinheim, 2012.

26. Lakowicz JR. Principles of Fluorescence Spectroscopy, 3rd edn. Springer: Berlin, 2006.
27. Jokanović V, Dramićanin MD, Andrić Ž. Nanodesigning of SiO2:Eu^{3+} particles obtained by spray pyrolysis method and their luminescence properties. Acta Chim Slov 2006; 53: 23–28.
28. Wan J, Jiang X, Li H, Chen K. Facile Synthesis of Zinc Ferrite nanoparticles as non-lanthanide T_1 MRI contrast agents. J Mater Chem 2012; 22: 13500–13505; doi: 10.1039/c2jm30684k
29. Truillet C, Lux F, Tillement O, Dugourd P, Antoine R. Coupling of HPLC with electrospray ionization mass spectrometry for studying the aging of ultrasmall multifunctional gadolinium-based nanoparticles. Anal Chem 2013; 85: 10440–10447; doi: 10.1021/ac402429p.
30. Le Duc G, Roux S, Paruta-Tuarez A, Dufort S, Brauer E, Marais A, Truillet C, Sancey L, Perriat P, Lux F, Tillement O. Advantages of gadolinium based ultrasmall nanoparticles vs molecular gadolinium chelates for radiotherapy guided by MRI for glioma treatment. Cancer Nano 2014; 5: 4.
31. Revheim ME, Roe K, Bruland OS, Bach-Gansmo T, Skretting A, Seierstad T. Monitoring the effect of targeted therapies in a gastrointestinal stromal tumor xenograft using a clinical PET/CT. Mol Imaging Biol 2011; 13: 1234–1240; doi: 10.1007/s11307-010-0464-0
32. Choi HS, Liu W, Misra P, Tanaka E, Zimmer JP, Ipe BI, Bawendi MG, Frangioni JV. Renal clearance of quantum dots. Nat Biotechnol 2007; 25: 1165–1170; doi: 10.1038/nbt1340
33. Kobayashi K, Brechbiel MW. Nano-sized MRI contrast agents with dendrimer cores. Adv Drug Deliver Rev 2005; 57: 2271–2286; doi: 10.1016/j.addr.2005.09.016
34. Longmire MR, Ogawa M, Choyke PL, Kobayashi H. Biologically optimized nanosized molecules and particles: more than just size. Bioconj Chem 2011; 22: 993–1000; doi: 10.1021/bc200111p
35. Evazalipour M, D'Huyvetter M, Soltani Tehrani B, Abolhassani M, Omidfar K, Abdoli S, Arezumand R, Morovvati H, Lahoutte T, Muyldermans S, Devoogdt N. Generation and characterization of nanobodies targeting PSMA for molecular imaging of prostate cancer. Contrast Media Mol Imaging 2014; 9: 211–220; doi: 10.1002/cmmi.1558

SUPPORTING INFORMATION

Additional supporting information may be found in the online version of this article at the publisher's web site.